ORIGINAL RESEARCH

Mechanisms of resistance to a PI3K inhibitor in gastrointestinal stromal tumors: an *omic* approach to identify novel druggable targets

Gloria Ravegnini[1,*]
Giulia Sammarini[1,*]
Sebastian Moran[2]
Giovanni Calice[3]
Valentina Indio[4]
Milena Urbini[4]
Annalisa Astolfi[4]
Federica Zanotti[1]
Maria A Pantaleo[4,5]
Patrizia Hrelia[1]
Sabrina Angelini[1]

[1]Department of Pharmacy and Biotechnology, University of Bologna, Bologna, Italy; [2]Cancer Epigenetics and Biology Program (PEBC), Bellvitge Biomedical Research Institue (Idibell), l'Hospitalet de Llobregat, Barcelona, Spain; [3]Laboratory of Preclinical and Translational Research, IRCCS-CROB, Referral Cancer Center of Basilicata, Rionero in Vulture, Italy; [4]Giorgio Prodi Cancer Research Center, University of Bologna, Bologna, Italy; [5]Department of Specialized, Experimental, and Diagnostic Medicine, Sant'Orsola-Malpighi Hospital, University of Bologna, Bologna, Italy

*These authors contributed equally to this work

Correspondence: Sabrina Angelini
Department of Pharmacy and Biotechnology, University of Bologna, 48 Via Irnerio, Bologna 40126, Italy
Tel +39 051 209 1787
Fax +39 051 209 1780
Email s.angelini@unibo.it

Background: Gastrointestinal stromal tumors (GISTs) represent a worldwide paradigm of target therapy. The introduction of tyrosine kinase inhibitors has deeply changed the prognosis of GIST patients, however, the majority of them acquire secondary mutations and progress. Unfortunately, besides tyrosine-kinase inhibitors, no other therapeutic options are available. Therefore, it is mandatory to identify novel molecules and/or strategies to overcome the inevitable resistance. In this context, after promising preclinical data on the novel PI3K inhibitor BYL719, the NCT01735968 trial in GIST patients who had previously failed treatment with imatinib and sunitinib started. BYL719 has attracted our attention, and we comprehensively characterized genomic and transcriptomic changes taking place during resistance.

Methods: For this purpose, we generated two in vitro GIST models of acquired resistance to BYL719 and performed an omic-based analysis by integrating RNA-sequencing, miRNA, and methylation profiles in sensitive and resistant cells.

Results: We identified novel epigenomic mechanisms of pharmacological resistance in GISTs suggesting the existence of pathways involved in drug resistance and alternatively acquired mutations. Therefore, epigenomics should be taken into account as an alternative adaptive mechanism.

Conclusion: Despite the fact that currently we do not have patients in treatment with BYL719 to verify this hypothesis, the most intriguing result is the involvement of H19 and PSTA1 in GIST resistance, which might represent druggable targets.

Keywords: gastrointestinal stromal tumors, GIST, BYL719, PI3K inhibitor, tyrosine-kinase inhibitors

Introduction

Gastrointestinal stromal tumors (GISTs) are rare mesenchymal tumors harboring *KIT*/*PDGFRA*-driver mutations in 85%–90% of cases.[1] GISTs are the example par excellence of targeted therapy in solid tumors. Indeed, with the introduction of the tyrosine-kinase inhibitor (TKI) imatinib, patients' prognosis have dramatically improved.[2] Despite imatinib effectiveness, the majority of patients with advanced GISTs have persistent measurable disease and eventually develop progressive disease within 24–36 months.[3] About 20 years after its approval, imatinib is still the gold standard in GIST treatment. However, to cope with the emergence of pharmacological resistance, the multi-TKIs sunitinib and regorafenib have been introduced, as second- and third-line treatment, respectively, in GIST management. Sunitinib and regorafenib share a mechanism of action with imatinib, adding

clinical benefit to GIST patients after imatinib failure. Even with clinical aids, the majority of patients experience tumor progression, due to the emergence of multiple drug–resistant *KIT/PDGFRA* mutations.[4–9] Unfortunately, all the approved treatments for GIST management are TKIs, and to date there are no additional therapeutic options. Therefore, the identification of novel druggable targets, favored by better characterization of the resistance process, may represent a key starting point to achieve a different clinical approach. In this regard, a novel PI3K inhibitor — BYL719 (Novartis) — is currently being tested in a phase IB trial in GIST patients who have previously failed imatinib and sunitinib (NCT01735968).[10] Specifically, BYL719 is a selective inhibitor of the PI3K catalytic p110a subunit.[11] Indeed, the PI3K pathway, which is downstream of *KIT/PDGFRA* receptors, is frequently activated in GIST and thought to be related to imatinib resistance.[12–16] Therefore, PI3K-pathway inhibition represents an attractive target and a promising strategy to counteract imatinib resistance in GIST. In this study, we comprehensively characterized genomic and transcriptomic changes taking place during resistance and how GIST cells evolve from being drug-sensitive to drug-resistant, from an "omic" point of view. For this purpose, we generated two in vitro GIST models of acquired resistance to BYL719 and performed an omic-based analysis by integrating RNA sequencing, miRNA profiling, and methylation profiling in sensitive and resistant cells.

Methods
Cell culture and treatment

Two established human imatinib-resistant GIST cell lines, GIST48 and GIST48B, were used (Table 1). These were authenticated by KIT-sequencing and TKI-sensitivity experiments, routinely grown in adhesion, and cultured at 37°C in a 5% CO_2 humidified atmosphere. To generate BYL719-resistant sublines, GIST48 and GIST48B were exposed to increasing concentrations of BYL719 (Selleck Chemicals, Houston, TX, USA), starting with a concentration of 0.05 μM and increasing gradually to 5 μM. Fresh drug was provided every 3–4 days, when the medium was replaced. After the cells had acquired the ability to grow in the presence of a specific concentration of BYL719, a proportion of them was frozen and the remaining grown at the next-highest drug level. After approximately 50 weeks, sublines of cells growing in 5 μM BYL719 were maintained continuously in culture at this dose. Upon receipt and before each change of BYL719 concentration, GIST lines were tested for mycoplasma contamination and were found to be negative.

IC$_{50}$: MTT-assay method

IC$_{50}$ was evaluated by MTT assays using a standard protocol.[17] Briefly, 10^4 cells/well were seeded in triplicate in a 96-well plate and incubated for 24 hours. After incubation, the medium was removed and replaced with a fresh one containing BYL719 in serial dilution and incubated for 48 hours. Subsequently, cells were washed with PBS and incubated with MTT (5 mg/mL) in PBS for 2 hours. Following MTT removal, the formazan crystals were dissolved in isopropanol and absorbance measured at 570 nm with a Tecan spectrophotometer (Spectra Model Classic, Salzburg, Austria).

DNA and RNA isolation

Genomic DNA and total RNA were extracted from parental (GIST48 and GIST48B) and BYL719-resistant (GIST48-R and GIST48B-R) cultured cells using the QIAamp DNA minikit and RNeasy minikit, respectively,

Table 1 GIST cell-lines [a] characteristics

	Origin	*KIT* mutations and other characteristics	Growth medium[b]
GIST48	GIST primary/patient[c]	Primary, homozygous *KIT* exon 11 (V560D) mutation; secondary, heterozygous *KIT* exon 17 (D820A[d]) mutation.	IMDM + 15% FBS
GIST48B	Subline of GIST48	Retains primary mutation (*KIT* V560D) in all cells; nearly undetectable *KIT* transcript and protein; secondary, heterozygous *KIT* exon 17 (D820A[d]) mutation; keeps downstream *KIT* signaling active	IMDM + 15% FBS

Notes: [a]Kindly provided by Dr Fletcher (Department of Pathology, Brigham and Women's Hospital, Harvard Medical School, Boston, MA); [b]reagents purchased from Thermo Fisher Scientific (Waltham, MA); [c]established from a GIST patient that had progressed after initial response to imatinib therapy; [d]located in the kinase-activation loop, confers resistance to imatinib and sunitinib.
Abbreviations: IMDM, Iscove's Modified Dulbecco's Medium; FBS, Fetal Bovine Serum.

following manufacturer's instructions. Both kits were purchased from Qiagen (Hilden, Germany).

KIT and PI3KCA mutational analysis

Genomic DNA from parental and BYL719-resistant cell lines was screened for the presence of hot-spot mutations in KIT (exons 9, 11 13, 14, 17, and 18) and PI3KCA (exons 9 and 20). Selected exons were amplified by PCR using specific primers. Amplified PCR products were purified and sequenced on both strands using a Big Dye Terminator version 1.1 cycle-sequencing kit (Thermo Fisher Scientific). Sanger sequencing was performed on an ABI 310 genetic analyzer (Applied Biosystems) and analyzed using Chromas (Technelysium). Sequencing data were analyzed using BLAST (https://blast.ncbi.nlm.nih.gov/Blast.cgi) to match sequences with reference sequences of KIT (NM_000222) and PI3KCA (NM_006218) genes obtained from Ensembl genome browser 94 (https://www.ensembl.org/index.html).

Western blot analysis

Whole-cell protein lysates were prepared from parental and BYL719-resistant cell-monolayers using NP40 buffer containing protease inhibitors (Halt protease- and phosphatase-inhibitor cocktail; Thermo Fisher Scientific) and 1 mM phenylmethylsulfonyl fluoride (Sigma-Aldrich). Proteins were separated on SDS-PAGE and transferred onto nitrocellulose membranes. Transfer efficiency was demonstrated by Ponceau S staining (Sigma-Aldrich). Membranes were blocked by 5% skimmed milk, followed by incubation at 4°C overnight with the presence of a primary antibody against KIT (A4502; Dako, Ely, UK), phospo-KIT (3391; Cell Signaling Technology, Leiden, Netherlands), AKT (9272; Cell Signaling Technology), phospo-AKT (9271; Cell Signaling Technology), MAPK (9102; Cell Signaling Technology), phospo-MAPK (9101; Cell Signaling Technology), mTOR (2972; Cell Signaling Technology), phospo-mTOR (2448; Cell Signaling Technology), PTEN (138G6; Cell Signaling Technology), and actin (A1978; Sigma-Aldrich). After rinsing, membranes were incubated with horseradish peroxidase–conjugated secondary antibody (Thermo Fisher Scientific) at room temperature for 2 hours. After further rinsing, immunoreactive bands were visualized by enhanced chemiluminescence (BioRad, Hercules, CA, USA) and signals captured and quantified using ChemiDoc (BioRad).

ABC transporter gene–expression analysis

Total RNA was reverse-transcribed to cDNA using a high capacity RNA-to-cDNA kit (Applied Biosystems) according to the manufacturer's instructions. cDNA was loaded into a TaqMan human ABC-transporter array, which allows quantitative gene-expression analysis of human ABC-transporter genes important in drug discovery and resistance. In particular, it contains assays in triplicate for 50 human genes and 14 endogenous controls in a 348-well array. mRNA-expression levels were normalized using GAPDH and 18S as endogenous controls, and data were analyzed using the $2^{-\Delta\Delta Ct}$ method. mRNAs with Ct>35 were considered unexpressed and excluded from further analysis.

RNA sequencing (RNA-seq)

Whole-transcriptome RNA libraries were prepared in accordance with the TruSeq RNA Sample Prep version 2 protocol (Illumina, San Diego, CA, USA). Poly(A)-RNA molecules from 500 ng total RNA were purified using oligo-dT magnetic beads. Subsequently, mRNA was fragmented and randomly primed for reverse transcription followed by second-strand synthesis to generate double-stranded cDNA fragments. The cDNA fragments generated went through a terminal end–repair process and ligation using paired-end sequencing adapters. The obtained products were amplified to enrich for fragments carrying adapters ligated on both ends, and to add additional sequences complementary to the oligonucleotides on the flow cell, thus creating the final cDNA library. 12pM paired-end libraries were amplified and ligated to the flow cell by bridge PC and sequenced at 2×75bp read length for RNA using Illumina sequencing-by-synthesis technology.

RNA-seq : bioinformatic analysis

After demultiplexing and FASTQ generation, through the bcltofastq function developed by Illumina, paired-end reads were trimmed using AdapterRemoval (https://github.com/MikkelSchubert/adapterremoval) with the aim of removing stretches of low-quality bases (<Q10) and Truseq/Nextera rapid-capture adapters present in the sequences. Sequences coming from RNA-seqwere mapped with TopHat/BowTie pipeline and PCR or optical duplicates were removed with the function rmdup of SAMtools.

RNA-seq: SNV calling

Single nucleotide variant (SNV) calling was performed with SAMtools and SNVMix2, which allows the identification of all point mutations and insertion/deletion variants. Variants in the dbSNP, 1000 Genomes, ExAc, and EVS databases with frequency >1% were excluded. The possible functional effects of identified variants were analyzed with three in silico tools: SIFT, PolyPhen2, and MutationTaster2.[18–20]

Gene-expression analysis

In order to compare gene-expression profile (GEP) between BYL719-sensitive and -resistant GIST cell lines, RNA-seq data were analyzed. After the alignment procedure, the BAM file obtained was manipulated with SAMtools to remove the optical/PCR duplicate and to sort and index it. The HTSeq count (Python HTSeq package) was adopted to count the number of reads mapped on known genes included in Ensembl 72 annotation features.

Functional annotation, GO, and pathway analysis

NetworkAnalyst (https://www.networkanalyst.ca/faces/home.xhtml) was used to identify molecular pathways and functional groupings. Gene-interaction networks, biofunction, and pathway analysis were generated using differentially expressed genes (DEGs) into known functions, pathways, and networks, primarily based on human studies. The DEGs were organized in Gene Ontology (GO) biofunction and regulatory effect networks. Significance was set at $P<0.05$. NetworkAnalyst uses a comprehensive high-quality protein–protein interaction database based on InnateDB. This database contains manually curated protein-interaction data from published literature, as well as experimental data from several protein–protein interaction databases, including IntAct, MINT, DIP, BIND, and BioGRID. The database currently contains 14,755 proteins and 145,955 interactions for humans.

qRT-PCR

Gene-expression levels of H19 and PSAT1 were evaluated through quantitative reverse-transcription (qRT) PCR. Briefly, RNA from both parental and BYL719-resistant cell lines was reverse-transcribed to cDNA using a high-capacity RNA-to-cDNA kit (Applied Biosystems) according to the manufacturer's instructions. qRT-PCR was performed with a Fast SYBR Green Master Mix (Applied Biosystems) using the 7900HT real-time PCR system. qRT-PCR assays for H19 and PSAT1 were performed using the primers H19-Fwd 5′-ATCGGTGCCTCAGCGTTCGG-3′, H19-Rev 5′-CTGTC CTCGCCGTCACACCG-3′, PSAT1-Fw 5′-ATACAGA GAATCTTGTGCGGG-3′, PSAT1-Rev 5′-CATAGTCAG CACACCTTCCTG-3′, GAPDH-Fwd 5′CGGGAAGCTT GTCATCAAT-3′, and GAPDH-Rev 5′-GACTCCACGAC GTACTCAGC-3′. All primers were obtained from Integrated DNA Technologies. Relative expression levels were evaluated by the $2^{-\Delta\Delta Ct}$ method using *GAPDH* as a housekeeping gene.

miRNA-expression evaluation

Total RNA (300 ng) was reverse-transcribed using a TaqMan miRNA reverse-transcription kit (Thermo Fisher Scientific) using Megaplex RT primers Human Pool A and Pool B. cDNAs were load on the TaqMan arrays Human MicroRNA A and B Cards and run on a 7900HT real-time PCR system in accordance with the manufacturer's procedure. miRNA data were analyzed with SDS relative quantification software version 2.4 (Applied Biosystems) and miRNAs with Ct>35 were considered unexpressed and excluded from further analysis. miRNA-expression levels were normalized using U6 and RNU48 as endogenous controls. Normalization was carried out by subtracting the mean Ct from individual Ct values. R-Bioconductor (package Limma) was adopted to evaluate differential expression profiles between the parental and BYL719-resistant GIST cell lines.

Global methylation profile

Genomic DNA (600 ng/sample) were bisulfite-converted using EZ DNA methylation kits (Zymo Research), and DNA methylation was measured using the Illumina Infinium HD-methylation assay with Infinium Methylation Epic BeadChips according to Illumina's protocol. Raw data (Idat files) were processed in R Bioconductor (minfi27). The quality of each sample was analyzed and probe signals removed when: i) $P>0.05$; ii) >1% of the data set contained no data; or iii) probes contained single-nucleotide polymorphisms. None of the samples included in the study was flagged as an outlier.[21] Statistical analyses were carried out using GenomeStudio, normalizing Idat values with controls provided by Illumina. The methylation score of each CpG is represented as a β-value, and differences between β-values of treated and untreated cells represent alterations in methylation level. The CpGs selected were those with absolute

methylation differential value of >0.2 or <–0.2.[21,22] To identify CpGs on promoter regions, we considered only UCSC reference-gene groups TSS200 or TSS1500.

Identification of validated miRNA targets

Targets of significant miRNAs were identified through specific in silico tools that allowed prediction of the most probable targets. Specifically, to limit false-positive results, we used the miRTarBase tool, which encloses more than 400,000 miRNA-target experimentally verified interactions, collected by manually surveying pertinent literature after systematic data mining of the text.

miRNA-profile and gene-expression correlation

miRNA and mRNA arrays were analyzed to highlight pairs of mRNAs and miRNAs that were discordant (up- versus downregulated and vice versa). Potential miRNA–mRNA interactions and miRNA/mRNA-expression profiles were used to construct functional interaction networks.

Methylation-profile and gene-expression correlation

To integrate methylation profiles and GEP, we considered only CpGs on promoter regions that shown absolute methylation differentials of >0.2 or <–0.2 in parental lines versus BYL719-resistant ones. Promoter regions were defined as upstream 1,500 bp and downstream 200 bp from the transcription-start site (TSS) of each gene. For each differentially methylated gene, we checked the expression level derived from RNA sequencing.

Results
MTT assay
GIST48 and GIST48B cell lines were exposed to BYL719 using doses that were increased in a stepwise manner. We thus established two BYL719-resistant GIST cell lines (48-R and 48B-R), which exhibited BYL719 IC$_{50}$ values that were about 15-fold higher than the parental cell lines (Figure S1).

KIT and PI3KCA mutational analysis

The involvement of *KIT* and *PI3KCA* mutations as mechanisms driving BYL719 resistance in GIST cells in vitro was investigated. Mutational analysis did not reveal additional *KIT* mutations in BYL719-resistant cell lines by Sanger sequencing or SNV calling. With regard to *PI3KCA*, we Sanger sequenced exons 9 and 20, both codifying for the catalytic p110a subunit and associated with drug resistance.[23–26] All samples were wild type. *PI3KCA* wild-type status was also confirmed by SNV calling.

Western blot analysis

To better characterize the BYL719-resistant GIST48-R and GIST48B-R lines, we performed Western blot analysis, evaluating in particular the signaling pathway downstream of *KIT* (Figure 1A). In the imatinib-resistant GIST48 line (as expected, considering that the targeted PI3K is downstream of *KIT*), we observed comparable *KIT* phosphorylation between GIST48 and GIST48B-R (Figure 1B). Absence of *KIT* phosphorylation was observed, as expected, in both GIST48B and GIST48B-R. Indeed this GIST model had entirely lost *KIT* expression (ie, KIT-negative, despite activation of downstream signaling [Figure 1C]). No differences were observed in PTEN status between parental and BYL719-resistant cell lines. On the contrary, in both GIST models, we detected activated AKT in BYL719-sensitive cell lines and inactivation in the resistant ones. We also observed activation of mTOR in both parental and BYL719-resistant cell lines. Finally, we observed MAPK activation in both BYL-sensitive and -resistant GIST models. All immunoblots are shown in Figure 1, B and C.

RNA-seq: SNV calling

We identified ten novel mutations in BYL719-resistant cells compared to parental cell lines. In particular, four mutations were identified in GIST48-R cells and six in GIST48B-R (Table 2). None of the mutations was common to both the two resistant GIST cell lines. With regard to GIST48-R, one mutation was identified as benign (*KIFC2*) and one probably damaging (*RPGR*) by the three tools. One mutation (*RIF1*) was predicted as probably damaging by two tools. Lastly, no agreement was reached for one mutation (*DPF1*). Concerning GIST48B-R, one mutation (*FRY*) was predicted as probably damaging by the three tools, two mutations (*PDGFB* and *SYT14*) were identified as benign by two tools, and no agreement was reached for two mutations (*DCHS1* and *EEF2KMT*). Lastly, one mutation (*RARS2*) was a gain of stop codon. Data are reported in Table 2. However, none of them was related to the PI3KCA pathway, had been previously identified in GIST, or associated with resistance in other tumor types; therefore, we did not consider them driver mutations for BYL719 resistance.
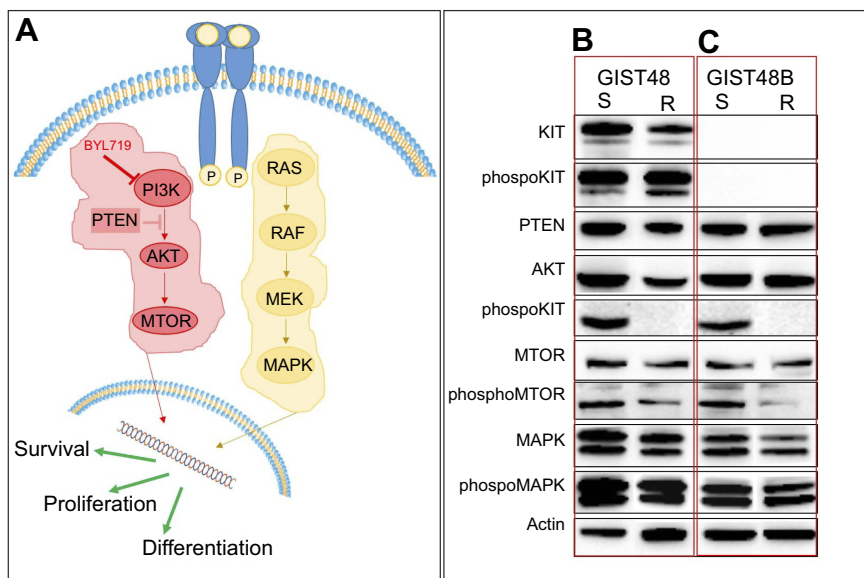
Figure 1 Western blot analysis.
Notes: (**A**) Simplified KIT-signaling pathway. Immunoblot evaluation of *KIT*, phospho-KIT, PTEN, AKT, phospho-AKT, mTOR, phospho-mTOR, MAPK, and phospho-MAPK in GIST48 (**B**) and GIST48B (**C**). S, BYL719-sensitive; R, BYL719-resistant.

Gene expression: ABC-transporter genes and RNA-seq analysis

Given the well-recognized role of ABC-transporter genes in mediating drug resistance, first we analyzed a custom panel of 50 genes in BYL719-sensitive and -resistant GIST lines. None was significantly deregulated. Therefore, we performed a RNA-seq analysis, which showed 95 differentially expressed genes with $P \leq 0.001$ and a false discovery rate <0.1 in BYL719-sensitive compared to BYL719-resistant GIST lines. In particular, 48 genes were upregulated, while 47 were downregulated. The significant DEGs are reported in Table S1. The 20 top deregulated genes — 13 up- and 7 downregulated — are shown in Figure 2A. GO functional enrichment analyses of deregulated genes showed cancer, chronic myeloid leukemia, and cell cycle as the top three deregulated pathways (Kyoto Encyclopedia of Genes and Genomes pathways (KEGG), Figure 2B). In addition, we found viral reproductive process and viral reproduction to be the top biological processes involved. RNA binding, structural constituents of ribosome, and structural molecular activity were the top three molecular functions. Finally, cytosol, macromolecular complex, and ribonucleoprotein complex were the top three cellular components involved. Interestingly, among the top upregulated genes in resistant cells, there was the long non coding RNA (lncRNA) H19. RNA-seq data were confirmed by qRT-PCR, which demonstrated overexpression of H19 in GIST48-R and GIST48B-R compared with the parental BYL719-sensitive lines, with fold changes of 20.8 and 6.9, respectively.

Table 2 Acquired mutations in BYL719-resistant GIST cells

GIST 48 vs GIST48-R				GIST 48B vs GIST48B-R			
Gene	**Exon**	**AA change**	**Prediction***	**Gene**	**Exon**	**AA change**	**Prediction***
DPF1	9	p.C313G	B[a], PD[c]	DCHS1	2	p.R168C	B[a], PD[b,c]
KIFC2	17	p.R732C	B[a–c]	EEF2KMT	2	p.H52Q	B[a,b], PD[c]
RIF1	19	p.V666A	PD[a,c]	FRY	5	p.D168Y	PD[a–c]
RPGR	6	p.Q171R	PD[a–c]	PDGFB	3	p.R51H	B[a,c]
				RARS2	1	p.C11X	Gain of stop codon[b]
				SYT14	6	p.V359A	B[b,c]

Note: *Prediction of the deleterious potential through [a]SIFT, [b]PolyPhen, and [c]MutationTaster2.
Abbreviations: AA, amino acid; B, benign; PD, probably damaging.
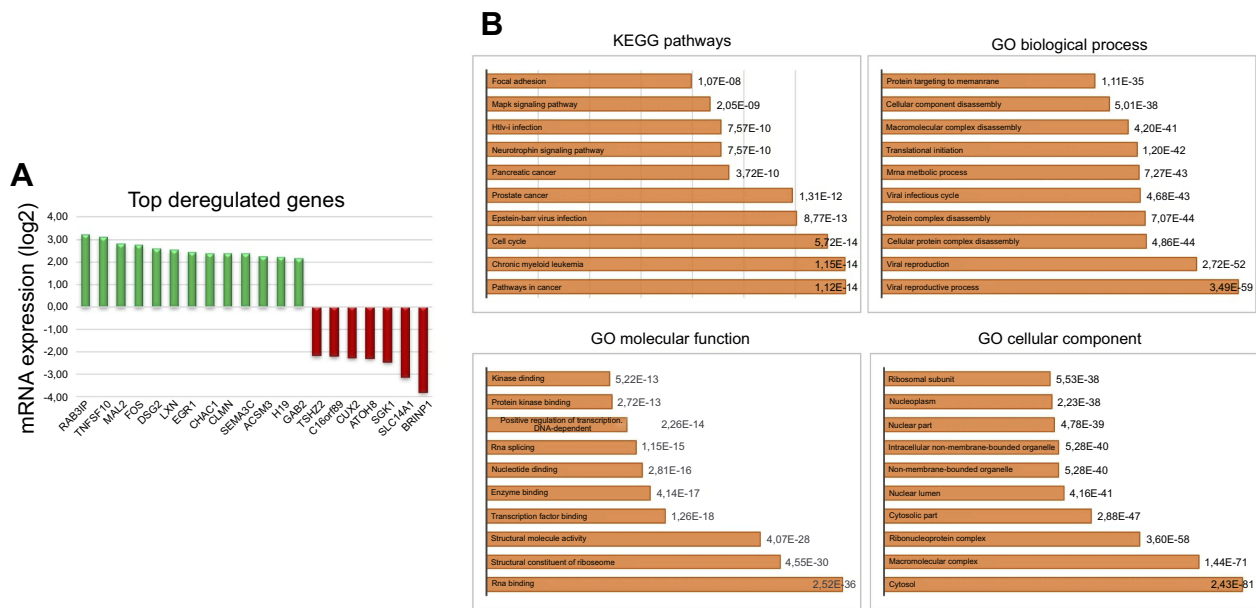
Figure 2 RNA-seq analysis.
Notes: (**A**) Top deregulated genes in BYL719-sensitive and -resistant GIST cell lines. (**B**) Go functional enrichment analysis of up- and downregulated genes.
Abbreviations: GIST, gastrointestinal stromal tumors; GO, gene ontology.

miRNA-expression profile

The array highlighted a total of 44 deregulated miRNAs of the 754 analyzed (P<0.05); however, after adjustment, only 13 miRNAs maintained statistical significance. In particular, two miRNAs — has-miR190b and has-miR299-5p — were upregulated and eleven miRNAs downregulated in resistant GIST cell lines compared to parental ones. All differentially expressed miRNAs are reported in Table 3. Hierarchical clustering of all samples dichotomized sensitive and resistant GIST cell lines into two distinct clusters (Figure 3A). Thr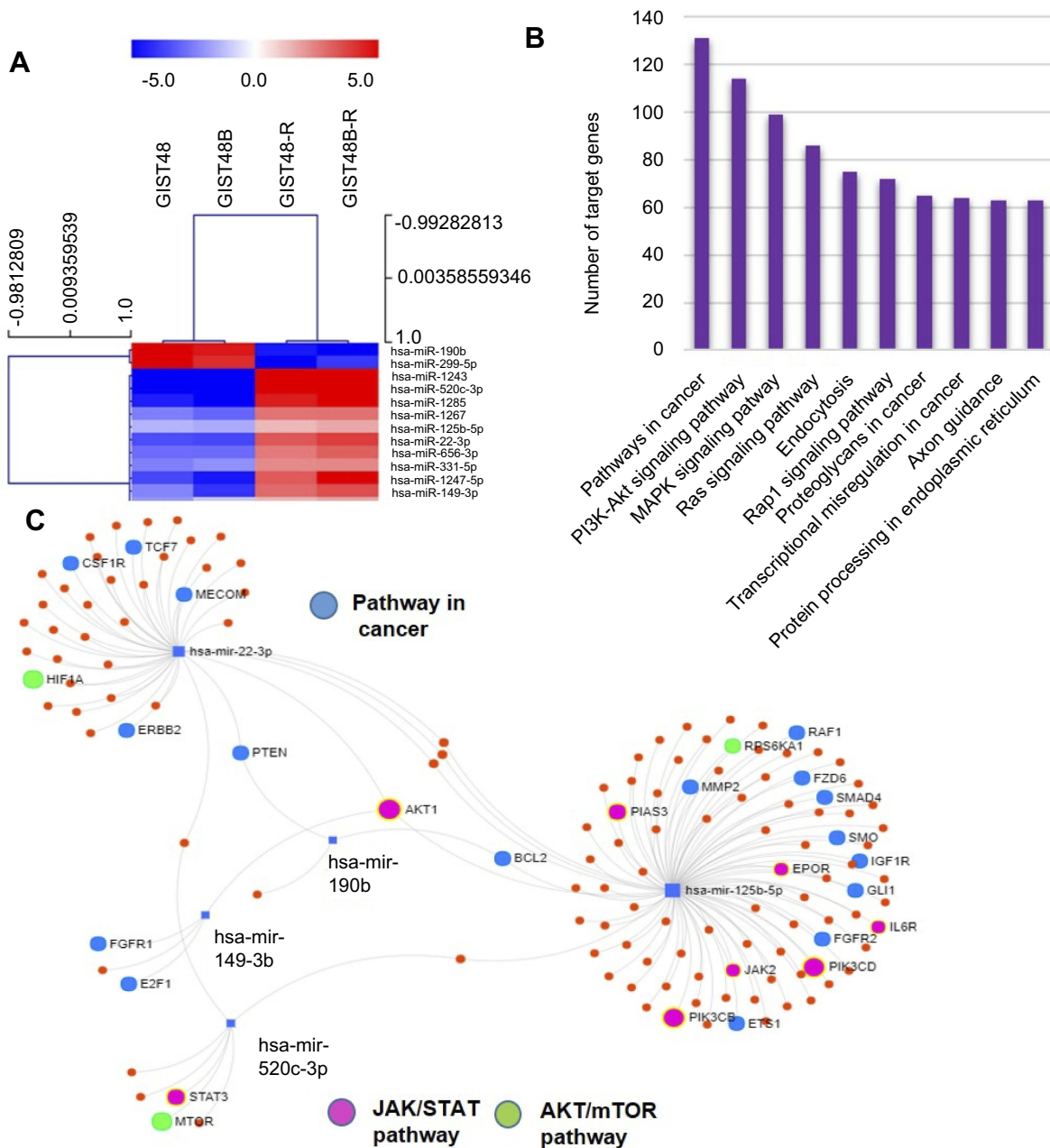ough miRPath 3.0, we assessed miRNA regulatory roles and identification of controlled pathways.[27] Interestingly, among the pathways potentially modulated by the deregulated miRNAs (summarized in Figure 3B), the most significant and those with the greatest number of target genes were PI3K/AKT, MAPK, and RAS cascades, which are involved in BYL719's mechanism of action. Figure 3C shows the main miRNAs involved in cancer (highlighted in blue) and PI3K–AKT (in green) and JAK–STAT (in pink) pathways. In particular, among the 13 deregulated miRNAs retrieved by our data, we identified a signature of five miRNAs mainly involved in the aforementioned pathways: miR22-3p, miR125b-5p, miR149-3p, miR190b, and miR520c-3p.

Global methylation profile

To determine whether acquired resistance involved modifications in DNA methylation, we performed genome-wide DNA-methylation profiling in BYL719-sensitive and -resistant GIST cell lines. We identified 3,305 differentially methylated CpGs. Among these, 2,817 were hypermethylated and 488 hypomethylated. Of the hypermethylated CpGs, 547 were in promoter regions of 379 genes, while 102 hypomethylated sites were in promoter regions of 70 genes. Unsupervised hierarchical cluster analysis of the demethylated genes divided the sensitive and resistant cell lines into two main clusters (Figure 4). Interestingly, as shown in Figure 5, A–C, the resistant cells showed significantly more hypermethylated CpG-island promoters compared to the sensitive counterparts.

Table 3 The most significantly deregulated miRNAs

miRNA	P-value	Adjusted P-value
hsa-miR1243	2.94^{-6}	0.002232799
hsa-miR520c-3p	1.27^{-5}	0.003316809
hsa-miR190b	1.31^{-5}	0.003316809
hsa-miR1289	2.72^{-5}	0.005164803
hsa-miR1247-5p	0.000118	0.016017348
hsa-miR22-3p	0.000126	0.016017348
hsa-miR1267	0.000188	0.020418143
hsa-miR299-5p	0.000237	0.022470219
hsa-miR125b-5p	0.000294	0.024789505
hsa-miR656-3p	0.000447	0.033993852
hsa-miR331-5p	0.000591	0.040837133
hsa-miR149-3p	0.000868	0.054998185
hsa-miR30d-5p	0.001126	0.065812471

Figure 3 miRNAs profile .
Notes: (**A**) miRNA hierarchical clustering. miRNAs identified as differentially expressed between BYL719-sensitive and -resistant GIST cell lines were selected as markers for unsupervised hierarchical clustering. (**B**) GO functional enrichment analysis of up- and downregulated miRNAs. (**C**) Main miRNAs involved in cancer (blue), AKT–mTOR (green) and JAK signaling cascades (pink) pathways.

miRNAs and mRNA network

To construct miRNA–DEG networks, we downloaded the experimentally verified associations between human miRNAs and their targets from miRTarBase. This data set consists of 4,076 miRNAs and 23,054 mRNAs,[28] and encloses more than 400,000 miRNA–target interactions collected by manually surveying pertinent literature after systematic data

mining of the text. Among the 13 deregulated miRNAs retrieved by our data, seven (miR331-5p, miR125b-5p, miR520c-3p, miR1289, miR299-5p, miR30d-5p, and miR149-3p) had verified associations with their targets. However, taking into account the canonical inverse correlation between miRNA and target expression, we were able to identify eight mRNA–miRNA networks. In particular, we found
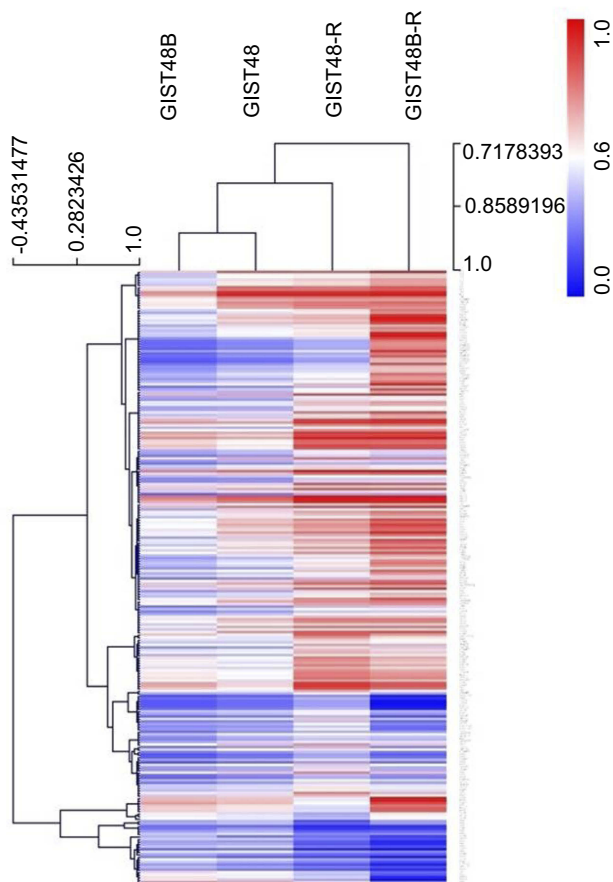
Figure 4 Global methylation profile.
Notes: Heat map showing DNA-methylation profiles in parental and BYL719-resistant cell lines ($\Delta\beta < -0.2$ or >0.2).

four miRNAs downregulated and the corresponding seven targets overexpressed (three miRNAs targeted two distinct mRNAs). One miRNA was upregulated and the corresponding target downregulated. The miRNAs and their corresponding targets are presented in Figure 6.

DNA methylation and mRNA network

To clarify the relationship between DNA methylation and differentially expressed mRNAs, we integrated the global methylation profile with DEGs. Results are shown in Figure 7. Among the genes with the strongest promoter hypermethylation and concomitant increased expression in resistant cells were *CLMN*, a member of the hedgehog-interacting protein family MAL, which encodes the T-lymphocyte maturation-associated protein and functions in T-cell differentiation. On the contrary, promoter hypermethylation and concomitant *TSHZ2* downregulation was observed, whereas *PSAT1* showed strong promoter

hypomethylation associated with increased gene expression after treatment. Overexpression of *PSAT1* was confirmed by qRT-PCR, which demonstrated overexpression of *PSAT1* in GIST48-R and GIST48B-R compared with the parental BYL719-sensitive lines, with fold changes of 4.1 and 5.8, respectively.

## Construction of the miRNA–mRNA–DNA methylation network

In order to identify a more comprehensive network, we integrated data deriving from GEP, miRNA, and methylation profiles. After intersection of all the data, the *PSAT1* gene was significantly upregulated in BYL719-resistant cell lines and showed promoter hypomethylation and a potential modulation by miR125b-5p (Figure 7).

Discussion

GISTs represent a worldwide paradigm of target therapy. The introduction of imatinib to clinical practice has deeply revolutionized its management, leading GISTs from an incurable disease to a sort of chronic disease. Imatinib has determined terrific improvement in GIST prognosis; however, as often happens with TKIs, the majority of patients acquire secondary mutations and the disease progresses. Unfortunately, no therapeutic options are available for patients who have failed on imatinib and the subsequent therapeutic lines: sunitinib and regorafenib. Therefore, it is pivotal and mandatory to identify novel molecules — different from TKIs — and/or strategies to overcome the inevitable resistance. In this context, after the promising preclinical data on the novel PI3K inhibitor BYL719,[10] the NCT01735968 trial in GIST patients who had previously failed treatment with imatinib and sunitinib started. BYL719 attracted our attention, and we comprehensively characterized genomic and transcriptomic changes taking place during resistance. Understanding how GIST cells evolve from being drug-sensitive to drug-resistant, from an omic point of view might accelerate the identification of novel druggable targets. For this purpose, we generated two in vitro GIST models of acquired resistance to BYL719 and performed an omic-based analysis by integrating RNA-seq, miRNA, and methylation profiling in sensitive and resistant cells. In particular, we selected GIST48 and GIST48B, sharing activation of *KIT* downstream signaling, including the PI3K pathway, targeted by BYL719.[29] Furthermore, both cell lines are resistant to the second-line treatment sunitinib,[30] making them
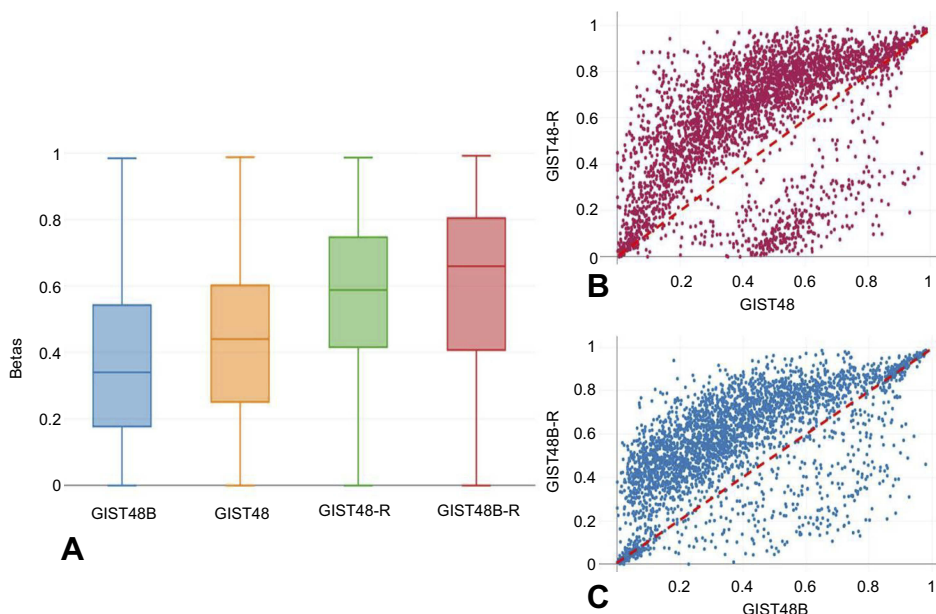
Figure 5 Global methylation profile.
Notes: (**A**) Box plots showing the β-values of CpGs islands at promoters only . General hypermethylation was more common in the BYL719-resistant cell lines. (**B, C**) Scatterplots of genome-wide DNA methylation levels (β). To highlight general hypermethylation, CpG islands with $\Delta\beta$<−0.2 or >0.2 are shown.
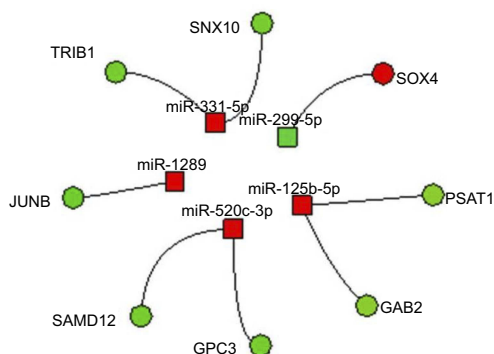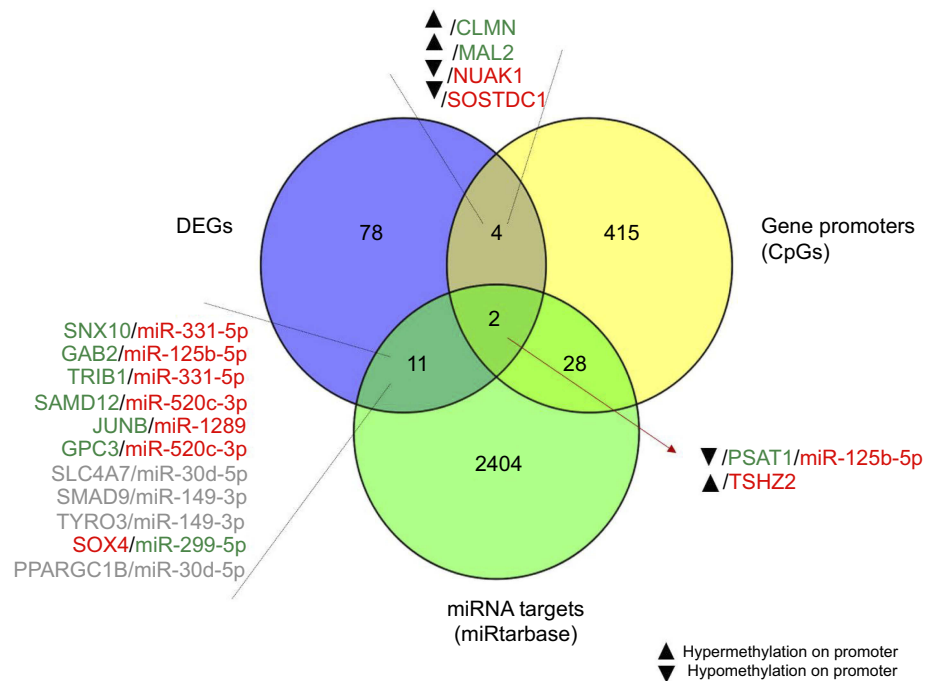

Figure 6 Integrated miRNA–mRNA regulatory networks.
Notes: Integration of GEP and miRNA profiles. Circles and squares represent genes and miRNAs, respectively. Red and green indicate downregulation and upregulation, respectively.
Abbreviation: GEP, gene expression profile.

good models, mirroring GIST patients who hypothetically will receive BYL719 treatment after imatinib and sunitinib failure.

TKI resistance is largely due to accumulation of additional kinase-domain mutations.[31] Therefore, we sequenced *KIT* and *PI3KCA* hot-spot exons — in addition to RNA-seq — to evaluate the appearance of novel point mutations or insertion/deletion variants possibly able to explain BYL719 resistance. Different alterations were found in BYL719-resistant lines; however, none was shared by both models, or harbored in *PI3KCA* and *KIT* genes, or downstream effectors. In addition, none of the mutated

genes has been involved in drug resistance; therefore, we did not consider them driver events for BYL719 unresponsiveness, pinpointing a potential novel mechanism of resistance in GISTs. Afterward, we analyzed a precast panel of 50 well-characterized ABC-transporter genes. Overexpression of genes involved in drug efflux is among the most common mechanisms of drug resistance.[32–34] However, we did not observe any significant difference in BYL719-resistant cell lines compared to sensitive ones. This prompted us to perform a more comprehensive gene-expression analysis through the RNA-seq approach. We identified the *H19* gene as one of the most significantly upregulated in BYL719-resistant cells compared to sensitive ones. *H19* has been described as an oncogenic lncRNA involved in cell proliferation, metastasis, epithelial–mesenchymal transition, and poor prognosis in several cancer types, including esophageal squamous-cell carcinoma, osteosarcoma, colorectal and gastric cancer, and others.[35–38]

A recent study reported H19 overexpression in GIST samples compared to normal paired tissue.[39] In addition, H19 upregulation showed a high correlation with ETV1 expression, which is crucial in GIST growth and survival. ETV1 cooperates with KIT through the MAPK-signaling pathway, and together they promote GIST tumorigenesis.[40] Furthermore, it has been reported that H19 might promote migration and invasion in colorectal cancer by activating the RAS protein and upregulating

▲ /CLMN
▲ /MAL2
▼ /NUAK1
▼ /SOSTDC1

DEGs

78

4

415

Gene promoters
(CpGs)

SNX10/miR-331-5p
GAB2/miR-125b-5p
TRIB1/miR-331-5p
SAMD12/miR-520c-3p
JUNB/miR-1289
GPC3/miR-520c-3p
SLC4A7/miR-30d-5p
SMAD9/miR-149-3p
TYRO3/miR-149-3p
SOX4/miR-299-5p
PPARGC1B/miR-30d-5p

2

11

28

2404

▼ /PSAT1/miR-125b-5p
▲ /TSHZ2

miRNA targets
(miRtarbase)

▲ Hypermethylation on promoter
▼ Hypomethylation on promoter

Figure 7 Integrated miRNA–mRNA–methylation regulatory networks.
Notes: Integration of GEP, miRNA, and methylation profiles. In gray are shown genes and miRNAs with the same trend of expression, which were excluded. Red and green indicate downregulation and upregulation, respectively.
Abbreviation: GEP, gene expression profile.

levels of phospho-RAF, phospho-MEK and phospho-MAPK.[41] Considering that RAS is upstream of both the PI3K and MAPK pathways,[42] this could represent an alternative mechanism through which resistant cells bypass PI3K and maintain their tumorigenic status. This assumption was confirmed by Western blot analysis, highlighting MAPK activation in both parental and BYL719-resistant cell lines. Interestingly, we also observed a weak activation of mTOR in BYL719-resistant cell lines, despite no AKT activity. This finding agrees with the recognized complex and dynamic cross talk between PI3K/AKT and MAPK.[43,44] Pathway cross talk allows a cell to achieve robust activation of key downstream targets or compensatory signaling. Particularly, the latter might be important in the context of drug resistance, allowing growth and viability of cancer cells. Indeed, combined inhibition of PI3K–Akt and MAPK pathways has shown efficacy in preclinical models,[43–46] and could be of interest in the management of imatinib-resistant GISTs.

Considering the lack of acquired *PI3KCA* mutations, we further evaluated the hypothesis that BYL719 resistance could be mediated by epigenetic mechanisms. Studies reported that epigenetic modifications may represent alternative mechanisms to evade

the pharmacological response.[47–49] In this context, different trials are evaluating epigenetic therapies as drug-resistance modulators in solid tumors.[47] With regard to GISTs, in recent years epigenetic treatments raised among the future perspective[50,51] alternatively to TKIs and/or to bypass TKI resistance. However, the results are still at an early stage, and further investigations are essential in this novel field. Consequently, we performed deep epigenomic characterization of these two in vitro models, looking for novel mechanisms of acquired resistance and potential druggable targets in GISTs. For this purpose, we performed miRNA profiling, identifying 13 miRNAs significantly deregulated in resistant cells. Among the pathways potentially modulated by these miRNAs, the most significant and those with the greatest number of target genes were PI3K/AKT–MAPK, and RAS cascades, which are involved in BYL719's mechanism of action. Subsequently, integration of miRNA arrays and GEP revealed five miRNAs targeting eight genes (*TRIB1*, *GAB2*, *SNX10*, *SAMD12*, *JUNB*, *GPC3*, and *SOX4*). Among those genes, *TRIB1* is a downstream effector of PI3K, and *GAB2*[52] cooperates with the PI3K–AKT pathway in promoting malignant behavior in cells.[53,54]

Subsequently, we integrated methylation and GEP, identifying two networks of interest involving *TSHZ2* and *PSAT1*. The *TSHZ2* gene resulted in downregulated BYL719-resistant cells compared to sensitive ones. TSHZ2, a zinc-finger homeobox nuclear protein, is supposed to be a tumor suppressor and is downregulated in breast cancer.[55] We speculated that TSHZ2 might bind transcriptional regulators that control the expression of crucial genes in tumorigenesis and resistance acquisition. Moreover, PSAT1 was upregulated in BYL719-resistant cells, and concomitant hypomethylation on the *PSAT1* promoter was found. However, on integration of miRNA and methylation profiles with gene-expression analysis, we pinpointed overexpression of PSAT1 associated with both promoter hypomethylation and miR125b-5p downregulation. In particular, PSAT1 overexpression in BYL719-resistant cell lines could represent an advantage for resistant cells, which have to find novel ploys to live.

Here, we showed that both methylation and miRNA modulated PSAT1 overexpression. Additional studies are needed to clarify if the epigenetic mechanisms act concurrently or in a mutual manner, with the final goal of increasing PSAT1 levels, which confer a metabolic-related growth advantage to tumor cells. PSAT1 overexpression is involved in drug resistance in different tumors, including colorectal cancer, melanoma, pancreatic cancer, and non-small-cell lung cancer.[56,57] PSAT1 belongs to the serine biosynthesis pathway, which has a key role in nucleotide and amino-acid metabolism. Levels of enzymes involved in serine synthesis have been shown to increase under conditions of DNA damage and genomic instability.[57,58] In addition, a recent study reported that serine supports one-carbon metabolism and proliferation of cancer cells.[59] Moreover, different evidence suggests that the serine pathway is crucial in cancer metabolism, using glycolysis-derived glucose for serine production and tumor growth.[60–64] In addition to these studies, which clearly ascribed to PSAT1 a role in tumorigenesis, a recent study on esophageal squamous-cell carcinoma patients linked PSAT1 overexpression to upregulation of the PI3K–AKT–GSK3β–Snail pathway.[65] Therefore, targeting PSAT1 might have potential therapeutic implication in GIST patients.

In conclusion, we identified novel epigenomic mechanisms of pharmacological resistance in GISTs, suggesting the existence of pathways involved in drug resistance and alternative to acquired mutations. We are aware that prolonged exposure and high BYL719 concentrations used to generate the resistant models can be de facto a substantial source of numerous off-target effects. However, prolonged inhibition of the PI3K pathway is probably accompanied by profound transcriptomic, proteomic, and metabolomic changes involved in drug resistance. Therefore, epigenomics should be taken into account as an alternative adaptive mechanism. Currently we do not have access to GIST patients in treatment with BYL719, and thus we are not able to verify the hypothesis in vivo. However, we consider these results intriguing, particularly the involvement of *H19* and *PSTA1* in GIST resistance, which might represent novel druggable targets for GIST patients.

Disclosure

The authors report no conflicts of interest in this work.

References

1. Mei L, Smith SC, Faber AC, et al. Gastrointestinal stromal tumors: the GIST of precision medicine. *Trends Cancer*. 2018;4(1):74–91. doi:10.1016/j.trecan.2017.11.006
2. Corless CL, Barnett CM, Heinrich MC. Gastrointestinal stromal tumours: origin and molecular oncology. *nat rev cancer*. 2011;11 (12):865–878. doi:10.1038/nrc3143
3. Serrano C, George S. Recent advances in the treatment of gastrointestinal stromal tumors. *Ther Adv Med Oncol*. 2014;6(3):115–127. doi:10.1177/1758834014522491
4. Demetri GD, van Oosterom AT, Garrett CR, et al. Efficacy and safety of sunitinib in patients with advanced gastrointestinal stromal tumour after failure of imatinib: a randomised controlled trial. *Lancet (London, England)*. 2006;368(9544):1329–1338. doi:10.1016/S0140-6736(06)69446-4
5. Demetri GD, Reichardt P, Kang Y-K, et al. Efficacy and Safety of regorafenib for advanced gastrointestinal stromal tumours after failure of imatinib and sunitinib (GRID): an international, multicentre, randomised, placebo-controlled, phase 3 trial. *Lancet*. 2013;381 (9863):295–302. doi:10.1016/S0140-6736(12)61857-1
6. Hemming ML, Heinrich MC, Bauer S, George S. Translational insights into gastrointestinal stromal tumor and current clinical advances. *Ann Oncol Off J Eur Soc Med Oncol*. 2018. doi:10.1093/ annonc/mdy309
7. Liegl B, Kepten I, Le C, et al. Heterogeneity of Kinase inhibitor resistance mechanisms in GIST. *J Pathol*. 2008;216(1):64–74. doi:10.1002/path.2382
8. Yoo C, Ryu M-H, Jo J, Park I, Ryoo B-Y, Kang Y-K. Efficacy of imatinib in patients with platelet-derived growth factor receptor alpha–mutated gastrointestinal stromal tumors. *Cancer Res Treat*. 2016;48 (2):546–552. doi:10.4143/crt.2015.015

9. Cassier PA, Fumagalli E, Rutkowski P, et al. Outcome of patients with platelet-derived growth factor receptor alpha-mutated gastrointestinal stromal tumors in the tyrosine kinase inhibitor era. *Clin Cancer Res*. 2012;18(16):4458–4464. doi:10.1158/1078-0432.CCR-11-3025

10. Van Looy T, Wozniak A, Floris G, et al. Phosphoinositide 3-kinase inhibitors combined with imatinib in patient-derived xenograft models of gastrointestinal stromal tumors: rationale and efficacy. *Clin Cancer Res*. 2014;20(23):6071–6082. doi:10.1158/1078-0432.CCR-14-1823

11. Fritsch C, Huang A, Chatenay-Rivauday C, et al. Characterization of the novel and specific PI3Kα inhibitor NVP-BYL719 and development of the patient stratification strategy for clinical trials. *Mol Cancer Ther*. 2014;13(5):1117–1129. doi:10.1158/1535-7163.MCT-13-0865

12. Serrano C, Wang Y, Mariño-Enríquez A, et al. KRAS and KIT gatekeeper mutations confer polyclonal primary imatinib resistance in GI stromal tumors: relevance of concomitant phosphatidylinositol 3-kinase/AKT dysregulation. *J Clin Oncol*. 2015;33(22):e93–6. doi:10.1200/JCO.2013.48.7488

13. Bauer S, Duensing A, Demetri GD, Fletcher JA. KIT oncogenic signaling mechanisms in imatinib-resistant gastrointestinal stromal tumor: PI3-kinase/AKT is a crucial survival pathway. *Oncogene*. 2007;26(54):7560–7568. doi:10.1038/sj.onc.1210558

14. Vivanco I, Sawyers CL. The phosphatidylinositol 3-kinase AKT pathway in human cancer. *Nat Rev Cancer*. 2002;2(7):489–501. doi:10.1038/nrc839

15. Patel S. Exploring novel therapeutic targets in GIST: focus on the PI3K/Akt/MTOR pathway. *Curr Oncol Rep*. 2013;15(4):386–395. doi:10.1007/s11912-013-0316-6

16. Ríos-Moreno MJ, Jaramillo S, Díaz-Delgado M, et al. Differential activation of MAPK and PI3K/AKT/MTOR pathways and IGF1R expression in gastrointestinal stromal tumors. *Anticancer Res*. 2011;31(9):3019–3025.

17. Ulukaya E, Colakogullari M, Wood EJ. Interference by anti-cancer chemotherapeutic agents in the MTT-tumor chemosensitivity assay. *Chemotherapy*. 2004;50(1):43–50. doi:10.1159/000077285

18. Kumar P, Henikoff S, Ng PC. predicting the effects of coding non-synonymous variants on protein function using the SIFT algorithm. *Nat Protoc*. 2009;4(7):1073–1081. doi:10.1038/nprot.2009.86

19. Adzhubei IA, Schmidt S, Peshkin L, et al. A method and server for predicting damaging missense mutations. *Nat Methods*. 2010;7 (4):248–249. doi:10.1038/nmeth0410-248

20. Schwarz JM, Cooper DN, Schuelke M, Seelow D. MutationTaster2: mutation prediction for the deep-sequencing age. *Nat Methods*. 2014;11(4):361–362. doi:10.1038/nmeth.2890

21. Barault L, Amatu A, Siravegna G, et al. Discovery of methylated circulating DNA biomarkers for comprehensive non-invasive monitoring of treatment response in metastatic colorectal cancer. *Gut*. 2017. doi:10.1136/gutjnl-2016-313372 gutjnl-2016-313372.

22. Moran S, Arribas C, Esteller M. Validation of a DNA methylation microarray for 850,000 cpg sites of the human genome enriched in enhancer sequences. *Epigenomics*. 2016;8(3):389–399. doi:10.2217/epi.15.114

23. Omarini C, Filieri ME, Bettelli S, et al. Mutational profile of metastatic breast cancer tissue in patients treated with exemestane plus everolimus. *Biomed Res Int*. 2018;2018:3756981. doi:10.1155/2018/3756981

24. Tessitore A, Bruera G, Mastroiaco V, et al. KRAS and 2 rare PI3KCA mutations coexisting in a metastatic colorectal cancer patient with aggressive and resistant disease. *Hum Pathol*. 2018;74:178–182. doi:10.1016/j.humpath.2018.01.021

25. Lai K, Killingsworth MC, Lee CS. Gene of the Month: *PIK3CA*. *J Clin Pathol*. 2015;68(4):253–257. doi:10.1136/jclinpath-2015-202885

26. Samuels Y, Wang Z, Bardelli A, et al. High frequency of mutations of the PIK3CA gene in human cancers. *Science*. 2004;304(5670):554. doi:10.1126/science.1096502

27. Vlachos IS, Zagganas K, Paraskevopoulou MD, et al. DIANA-MiRPath v3.0: deciphering MicroRNA function with experimental support. *Nucleic Acids Res*. 2015;43(W1):W460–W466. doi:10.1093/nar/gkv403

28. Chou C-H, Shrestha S, Yang C-D, et al. MiRTarBase update 2018: a resource for experimentally validated MicroRNA-target interactions. *Nucleic Acids Res*. 2018;46(D1):D296–D302. doi:10.1093/nar/gkx1067

29. Mühlenberg T, Zhang Y, Wagner AJ, et al. Inhibitors of deacetylases suppress oncogenic KIT signaling, acetylate HSP90, and induce apoptosis in gastrointestinal stromal tumors. *Cancer Res*. 2009;69 (17):6941–6950. doi:10.1158/0008-5472.CAN-08-4004

30. Heinrich MC, Maki RG, Corless CL, et al. Primary and secondary kinase genotypes correlate with the biological and clinical activity of sunitinib in imatinib-resistant gastrointestinal stromal tumor. *J Clin Oncol*. 2008;26(33):5352–5359. doi:10.1200/JCO.2007.15.7461

31. Wardelmann E, Merkelbach-Bruse S, Pauls K, et al. Polyclonal evolution of multiple secondary KIT mutations in gastrointestinal stromal tumors under treatment with imatinib mesylate. *Clin Cancer Res*. 2006;12(6):1743–1749. doi:10.1158/1078-0432.CCR-05-1211

32. Beretta GL, Cassinelli G, Pennati M, Zuco V, Gatti L. Overcoming ABC transporter-mediated multidrug resistance: the dual role of tyrosine kinase inhibitors as multitargeting agents. *Eur J Med Chem*. 2017;142:271–289. doi:10.1016/j.ejmech.2017.07.062

33. Choi YH, Yu A-M. ABC transporters in multidrug resistance and pharmacokinetics, and strategies for drug development. *Curr Pharm Des*. 2014;20(5):793–807. doi:10.2174/138161282005140214165212

34. Klukovits A, Krajcsi P. Mechanisms and therapeutic potential of inhibiting drug efflux transporters. *Expert Opin Drug Metab Toxicol*. 2015;11(6):907–920. doi:10.1517/17425255.2015.1028917

35. Raveh E, Matouk IJ, Gilon M, Hochberg A. The H19 long non-coding RNA in cancer initiation, progression and metastasis - a proposed unifying theory. *Mol Cancer*. 2015;14(1):184. doi:10.1186/s12943-015-0458-2

36. Huarte M. The emerging role of LncRNAs in cancer. *Nat Med*. 2015;21(11):1253–1261. doi:10.1038/nm.3981

37. Yang Q, Wang X, Tang C, Chen X, He J. H19 promotes the migration and invasion of colon cancer by sponging MiR-138 to upregulate the expression of HMGA1. *Int J Oncol*. 2017;50(5):1801–1809. doi:10.3892/ijo.2017.3941

38. Li H, Yu B, Li J, et al. Overexpression of LncRNA H19 enhances carcinogenesis and metastasis of gastric cancer. *Oncotarget*. 2014;5 (8):2318–2329. doi:10.18632/oncotarget.1913

39. Xue L, Wang Y, Yue S, Zhang J. The expression of miRNA-221 and miRNA-222 in gliomas patients and their prognosis. *Neurol Sci*. 2017;38(1):67–73. doi:10.1007/s10072-016-2710-y

40. Chi P, Chen Y, Zhang L, et al. ETV1 is a lineage survival factor that cooperates with KIT in gastrointestinal stromal tumours. *Nature*. 2010;467(7317):849–853. doi:10.1038/nature09409

41. Yang W, Redpath R, Zhang C, Ning N. Long non-coding RNA H19 promotes the migration and invasion of colon cancer cells via MAPK signaling pathway. *Oncol Lett*. 2018;16(3):3365–3372. doi:10.3892/ol.2018.9052

42. Tolcher AW, Peng W, Calvo E. Rational approaches for combination therapy strategies targeting the MAP kinase pathway in solid tumors. *Mol Cancer Ther*. 2018;17(1):3–16. doi:10.1158/1535-7163.MCT-17-0349

43. Aksamitiene E, Kiyatkin A, Kholodenko B.N. Cross-talk between mitogenic Ras/MAPK and survival PI3K/Akt pathways: a fine balance. *Biochem Soc Trans*. 2012;40(5):139–146. doi:10.1042/BST20110609

44. Alonso N, Diaz Nebreda A, Monczor F, et al. PI3K pathway is involved in ERK signaling cascade activation by histamine H2R agonist in HEK293T cells. *Biochim Biophys Acta*. 2016;1860 (9):1998–2007. doi:10.1016/j.bbagen.2016.06.016

45. Serra V, Scaltriti M, Prudkin L, et al. PI3K Inhibition Results in Enhanced HER Signaling and Acquired ERK Dependency in HER2-Overexpressing Breast Cancer. *Oncogene*. 2011;30 (22):2547–2557. doi:10.1038/onc.2010.626

46. Engelman JA, Chen L, Tan X, et al. Effective use of PI3K and MEK inhibitors to treat mutant kras G12D and PIK3CA H1047R murine lung cancers. *Nat Med*. 2008;14(12):1351–1356. doi:10.1038/nm.1890

47. Brown R, Curry E, Magnani L, Wilhelm-Benartzi CS, Borley J. Poised epigenetic states and acquired drug resistance in cancer. *Nat Rev Cancer*. 2014;14(11):747–753. doi:10.1038/nrc3819

48. Knoechel B, Roderick JE, Williamson KE, et al. An epigenetic mechanism of resistance to targeted therapy in T cell acute lymphoblastic leukemia. *Nat Genet*. 2014;46(4):364–370. doi:10.1038/ng.2913

49. Salgia R, Kulkarni P. The genetic/non-genetic duality of drug 'resistance' in cancer. *Trends Cancer*. 2018;4(2):110–118. doi:10.1016/j.trecan.2018.01.001

50. Nervi C, De Marinis E, Codacci-Pisanelli G. Epigenetic treatment of solid tumours: a review of clinical trials. *Clin Epigenetics*. 2015;7:127. doi:10.1186/s13148-015-0157-2

51. Bauer S, Hilger RA, Mühlenberg T, et al. Phase I study of panobinostat and imatinib in patients with treatment-refractory metastatic gastrointestinal stromal tumors. *Br J Cancer*. 2014;110 (5):1155–1162. doi:10.1038/bjc.2013.826

52. De Marco C, Laudanna C, Rinaldo N, et al. Specific Gene expression signatures induced by the multiple oncogenic alterations that occur within the PTEN/PI3K/AKT pathway in lung cancer. *PLoS One*. 2017;12(6):e0178865. doi:10.1371/journal.pone.0178865

53. Wang Y, Sheng Q, Spillman MA, Behbakht K, Gu H. Gab2 regulates the migratory behaviors and e-cadherin expression via activation of the pi3k pathway in ovarian cancer cells. *Oncogene*. 2012;31 (20):2512–2520. doi:10.1038/onc.2011.435

54. Wang WJ, Mou K, Wu XF, et al. Grb2-associated binder 2 silencing impairs growth and migration of H1975 cells via modulation of PI3K-Akt signaling. *Int J Clin Exp Pathol*. 2015;8 (9):10575–10584.

55. Yamamoto M, Cid E, Bru S, Yamamoto F. Rare and frequent promoter methylation, respectively, of TSHZ2 and 3 genes that are both downregulated in expression in breast and prostate cancers. *PLoS One*. 2011;6(3):e17149. doi:10.1371/journal.pone.0017149

56. Vié N, Copois V, Bascoul-Mollevi C, et al. Overexpression of phosphoserine aminotransferase PSAT1 stimulates cell growth and increases chemoresistance of colon cancer cells. *Mol Cancer*. 2008;7(1):14. doi:10.1186/1476-4598-7-14

57. Ross KC, Andrews AJ, Marion CD, Yen TJ, Bhattacharjee V. Identification of the serine biosynthesis pathway as a critical component of BRAF inhibitor resistance of melanoma, pancreatic, and non–small cell lung cancer cells. *Mol Cancer Ther*. 2017;16 (8):1596–1609. doi:10.1158/1535-7163.MCT-16-0798

58. Markkanen E, Fischer R, Ledentcova M, Kessler BM, Dianov GL. Cells deficient in base-excision repair reveal cancer hallmarks originating from adjustments to genetic instability. *Nucleic Acids Res*. 2015;43(7):3667–3679. doi:10.1093/nar/gkv222

59. Labuschagne CF, van Den Broek NJF, Mackay GM, Vousden KH, Maddocks ODK. Serine, but not glycine, supports one-carbon metabolism and proliferation of cancer cells. *Cell Rep*. 2014;7 (4):1248–1258. doi:10.1016/j.celrep.2014.04.045

60. Schulze A, Harris AL. How cancer metabolism is tuned for proliferation and vulnerable to disruption. *Nature*. 2012;491 (7424):364–373. doi:10.1038/nature11706

61. Luo J. Cancer's sweet tooth for serine. *Breast Cancer Res*. 2011;13 (6):317. doi:10.1186/bcr2932

62. De Marchi T, Timmermans MA, Sieuwerts AM, et al. Phosphoserine aminotransferase 1 is associated to poor outcome on tamoxifen therapy in recurrent breast cancer. *Sci Rep*. 2017;7(1):2099. doi:10.1038/s41598-017-02296-w

63. Locasale JW, Grassian AR, Melman T, et al. Phosphoglycerate dehydrogenase diverts glycolytic flux and contributes to oncogenesis. *Nat Genet*. 2011;43(9):869–874. doi:10.1038/ng.890

64. Possemato R, Marks KM, Shaul YD, et al. Functional genomics reveal that the serine synthesis pathway is essential in breast cancer. *Nature*. 2011;476(7360):346–350. doi:10.1038/nature10350

65. Liu B, Jia Y, Cao Y, et al. Overexpression of phosphoserine aminotransferase 1 (PSAT1) predicts poor prognosis and associates with tumor progression in human esophageal squamous cell carcinoma. *Cell Physiol Biochem*. 2016;39(1):395–406. doi:10.1159/000445633

Supplementary materials

Table S1 List of genes differentially expressed in parental and resistant cell lines

Upregulated genes in BYL719-resistant cell lines				Downregulated genes in BYL719-resistant cell lines			
	LogFC	*P*-value	FDR		LogFC	*P*-value	FDR
H19	2.23	8.61^{-12}	1.08^{-7}	C16ORF89	−2.21	0	0.000001
RAB3IP	3.23	1.19^{-9}	3.93^{-6}	MXRA5	−1.90	0	0.000004
ANXA3	1.81	8.24^{-8}	0.000148	BRINP1	−3.82	0	0.000121
LXN	2.57	2.9^{-7}	0.000304	CUX2	−2.27	0	0.000215
CHAC1	2.41	1^{-6}	0.000841	SLC4A7	−1.57	0	0.000215
TNFSF10	3.12	1.53^{-6}	0.001043	PCSK6	−1.78	0	0.000215
CLMN	2.40	1.8^{-6}	0.001078	SGK1	−2.46	0.000001	0.000535
ACSM3	2.26	5.71^{-6}	0.002987	GPC2	−1.79	0.000001	0.001010
PDE5A	1.52	9.67^{-6}	0.004328	FN1	−1.54	0.000003	0.001451
DSG2	2.60	1.39^{-5}	0.005618	RHBDF1	−1.43	0.000007	0.003245
ASNS	1.30	1.58^{-5}	0.00619	SAMD11	−1.38	0.000008	0.003622
PSAT1	1.48	1.96^{-5}	0.007033	VCAM1	−1.67	0.000017	0.006486
SNX10	2.00	2.51^{-5}	0.008495	ID3	−1.69	0.000019	0.006898
LMO4	1.29	2.64^{-5}	0.008495	SMAD9	−1.28	0.000029	0.008963
SEMA3C	2.39	3^{-5}	0.009034	SLC14A1	−3.15	0.000030	0.009034
GLRB	2.02	3.22^{-5}	0.009306	TSHZ2	−2.18	0.000033	0.009306
ADD2	1.62	4.99^{-5}	0.012541	MME	−1.47	0.000035	0.009897
EGR1	2.46	7.05^{-5}	0.017026	RP11-54O7.1	−2.01	0.000041	0.010885
MAL2	2.82	7.84^{-5}	0.017893	PHF2P2	−1.39	0.000042	0.011066
PRIMA1	2.06	8.88^{-5}	0.018896	TYRO3	−1.42	0.000097	0.019908
TBC1D2B	1.47	9.25^{-5}	0.019348	NUAK1	−1.45	0.000105	0.020765
GAB2	2.19	0.000108	0.020816	PHLDB2	−1.64	0.000106	0.020765
PROCR	1.89	0.000129	0.023094	DACT3	−1.43	0.000104	0.020765
ICA1	2.05	0.000132	0.023302	GTF2IP3	−2.01	0.000109	0.020816
PRKCQ-AS1	1.56	0.000142	0.024358	ID2	−1.25	0.000117	0.021688
DOCK9	1.77	0.000171	0.0276	EFNB2	−1.59	0.000137	0.023811
LAMP3	1.22	0.000232	0.035097	IQGAP2	−1.14	0.000144	0.024358
TRIB1	1.25	0.000232	0.035097	RBM18	−1.17	0.000170	0.027600
TBC1D8B	1.62	0.000266	0.038374	SOSTDC1	−1.84	0.000189	0.030100
SFRP1	1.10	0.000358	0.048283	F2R	−1.48	0.000225	0.034926
TNFAIP8	1.29	0.000407	0.052689	ADGRD1	−1.54	0.000262	0.038374
SAMD12	2.06	0.000424	0.053714	GAREM	−1.46	0.000297	0.042399
JUNB	1.43	0.000444	0.055782	SOX4	−1.23	0.000306	0.043207
DAAM2	1.21	0.000483	0.05878	SMAD6	−1.21	0.000350	0.047754
IGSF3	1.13	0.000487	0.05878	SH3BP5-AS1	−1.66	0.000347	0.047754
LGI2	1.90	0.000521	0.061597	PREX2	−1.06	0.000369	0.049242
CALB2	1.72	0.000525	0.061597	BCRP3	−1.76	0.000420	0.053714
PDE3B	1.39	0.000552	0.063588	COL16A1	−1.15	0.000449	0.055782
GPC3	1.71	0.000574	0.064953	PDLIM3	−1.45	0.000463	0.056947
TNFRSF19	2.17	0.000571	0.064953	ADAMTS2	−1.65	0.000512	0.061195
FOXP2	1.57	0.00061	0.06843	WTIP	−1.16	0.000531	0.061674
BST2	1.18	0.000619	0.068795	MYO1B	−1.27	0.000626	0.068960
HUNK	1.30	0.000647	0.070631	SORBS1	−1.55	0.000703	0.075396
FAM19A4	1.76	0.000709	0.075396	PPARGC1B	−1.01	0.000794	0.081682
ARRB1	1.27	0.000737	0.07712	ATOH8	−2.31	0.000808	0.082507
CCDC181	1.55	0.000893	0.088251	ZDHHC11	−1.33	0.000832	0.084194
GLTSCR2	0.98	0.001004	0.098527	CTGF	−1.16	0.000869	0.087235
FOS	2.77	0.001014	0.098663				

Abbreviation: FDR, fold discovery rate.
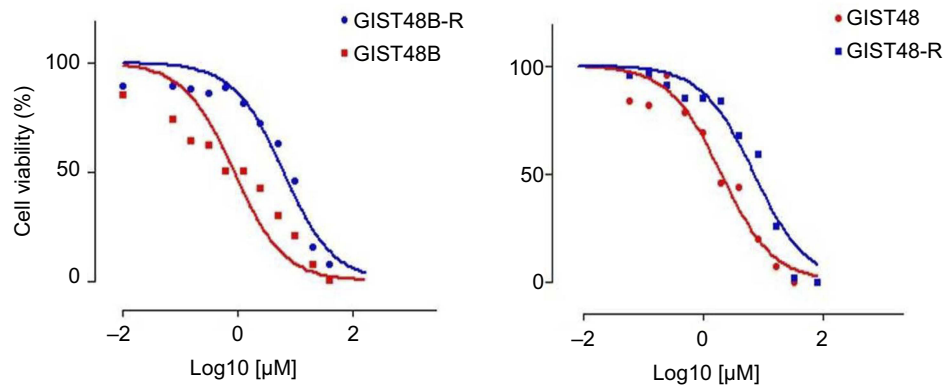
Figure S1 MTT assay.
Notes: Cell viability in GIST48 and GIST48B (red curves) and BYL719-resistant counterparts (blue curves).